2018

# A Visualization Investigation on the Influence of the Operating Conditions on the Phase Change in the Primary Convergent-divergent Nozzle of a Transcritical CO2 Ejector

Yafei Li
*School of Chemical Engineering and Technology, Xi'an Jiaotong University, Xi'an 710049, Shaanxi, People's Republic of China*, lyfxjtu@stu.xjtu.edu.cn

Jianqiang Deng
*School of Chemical Engineering and Technology, Xi'an Jiaotong University, China.*, dengjq@mail.xjtu.edu.cn

Li Ma
*School of Chemical Engineering and Technology, Xi'an Jiaotong University, Xi'an 710049, Shaanxi, People's Republic of China*, xjtuhgmali@stu.xjtu.edu.cn

Yang He
*School of Chemical Engineering and Technology, Xi'an Jiaotong University, Xi'an 710049, Shaanxi, People's Republic of China*, hywwym@mail.xjtu.edu.cn

# A Visualization Investigation on the Influence of the Operating Conditions on the Phase Change in the Primary Convergent-divergent Nozzle of a Transcritical $CO_2$ Ejector

Yafei LI[1], Jianqiang DENG[2]*, Li MA[3], Yang HE[4]

[1] Xi'an Jiaotong University, School of Chemical Engineering and Technology, Xi'an, Shaanxi, China
Email: lyfxjtu@stu.xjtu.edu.cn

[2] Xi'an Jiaotong University, School of Chemical Engineering and Technology, Xi'an, Shaanxi, China
Tel.: +86-029-82663413, Fax: +86-029-82663413, Email: dengjq@mail.xjtu.edu.cn

[3] Xi'an Jiaotong University, School of Chemical Engineering and Technology, Xi'an, Shaanxi, China
Email: xjtuhgmali@stu.xjtu.edu.cn

[4] Xi'an Jiaotong University, School of Chemical Engineering and Technology, Xi'an, Shaanxi, China
Email: hywwym@mail.xjtu.edu.cn

* Corresponding Author

## ABSTRACT

Complex flow processes exist in the primary convergent-divergent nozzle of a transcritical $CO_2$ ejector because of the rapid expansion of supercritical $CO_2$ flow, which has a significant influence on the performance of a transcritical $CO_2$ ejector expansion refrigeration system. A visualization experiment with the direct photography method was carried out to investigate the phase change phenomena in the primary convergent-divergent nozzle of a transcritical $CO_2$ ejector. The visualization transcritical $CO_2$ ejector was designed as a rectangular cross-section to minimize the optical distortion. In order to better interpret the phase change phenomena of $CO_2$ flow, four pressure measurement points were lumped in the convergent-divergent nozzle to get the pressure distribution along the convergent-divergent nozzle for various operating conditions. The results revealed that the phase change position in the convergent-divergent nozzle was closely related to the primary flow inlet conditions and the suction flow inlet pressure. The results showed that the phase change could start after or before the nozzle throat, and the phase change position moved upstream by decreasing the primary flow inlet pressure and temperature simultaneously. As keeping the primary flow inlet pressure constant, the phase change position also moved upward by decreasing the suction flow inlet pressure. In addition, the measured pressure results indicated that the pressure differences in the convergent section of the primary convergent-divergent nozzle increased as the $CO_2$ suction flow inlet pressure decreased because of more adequate expansion of the primary flow.

## 1. INTRODUCTION

The ejector is used in a transcritical $CO_2$ ejector expansion refrigeration cycle (EERC) to recover the throttling losses and reduce the compressor powers, which is considered as a promising technique to improve the system coefficient of performance (COP) (Elbel and Lawrence, 2016; Besagni *et al*., 2016). The superiority of using the ejector to improve the system performance has been claimed based on theoretical and experimental investigations. Li and Groll (2004) proposed a constant pressure mixing model on the ejector and pointed out that the COP could be

improved by more than 16% over the conventional transcritical $CO_2$ vapor compression refrigeration cycle (VCRC). Deng *et al*. (2007) presented a thermodynamic analysis and showed that the maximum COP of the EERC was 22.0% better than the VCRC, and the cooling capacity could be improved by 11.5%. Ahammed *et al*. (2014) implemented a numerical simulation on the EERC, and their results revealed a COP improvement of 21% compared to an equivalent conventional $CO_2$ system. The experimental investigation of Elbel and Hrnjak (2008) indicated that COP of EERC could be improved by 7%, and the cooling capacity could be enhanced by 8% compared to the conventional $CO_2$ system. Lee *et al*. (2011) carried out an experimental study on the performance improvement of EERC, and they stated that the COP was about 15% higher than that of the conventional system at given conditions. Liu *et al*. (2012) designed an adjustable ejector for the EERC and found that the adjustable ejector can significantly improve the COP according to their experimental results.

Besides investigating the EERC system performance, the complex flow phenomena in an ejector also attracted increasing interests in the recent decade. Flow visualization methods and internal pressure and temperature measurement approaches have been successfully applied to investigate the flow field structure of the ejector. Bouhanguel *et al*. (2011) experimentally studied the shock structure, mixing process, turbulent structures and flow instability in a supersonic air ejector with laser tomography techniques. Rao and Jagadeesh (2014) employed the time resolved schlieren and laser scattering visualization technique to observe the mixing process of a supersonic air ejector, and visualization images showed that the non-mixed length was 4.5 to 5.2 times the height of the mixing duct. Little and Garimella (2016) visualized the condensation phenomena in a two-phase R134a ejector using the shadowgraph method. However, it is notoriously difficult to conduct a visualization experiment on a transcritical $CO_2$ ejector because of the higher pressure compared with those low-pressure ejectors. Zhu *et al*. (2017) used the direct photography method to investigate the primary flow expansion angles and mixing phenomenon in a transcritical $CO_2$ ejector for various operating conditions. The flow phenomena in the primary nozzle were not investigated in their experiment due to the limitation of the visualization window. Moreover, it is difficult to measure the static pressure and temperature in high-speed flows, particularly in the supersonic flow. Nakagawa *et al*. (2009) obtained the pressure and temperature values along the diverging section of several supersonic $CO_2$ primary converging-diverging nozzles with thermocouples and strain-gauges. The pressure distribution along the converging section was not measured in their experiment. Elbel (2011) measured wall static pressure distribution of a transcritical $CO_2$ two-phase ejector.

In contrast to the investigations on the performance improvement of the transcritical $CO_2$ ejector expansion system, the visualization study on the transcritical $CO_2$ two-phase ejector is not sufficient, and the internal flow characteristics are too complicated to be well understood so far, especially in the primary nozzle. The purpose of this research is to combine the visualization method and pressure measurement method to investigate the phase change phenomena in the primary convergent-divergent nozzle of a transcritical $CO_2$ two-phase ejector. The position of phase change and pressure distribution along the nozzle were investigated for various operating conditions.

## 2. EXPERIMENTAL SETUP

### 2.1 Experimental System

The schematic diagram of the transcritical $CO_2$ ejector expansion cycle used in the experiment is illustrated in Figure 1. The cycle can be divided into a high-pressure sub-cycle and a low-pressure sub-cycle. The high-pressure sub-cycle mainly consists of a compressor, a gas cooler, an ejector and a gas-liquid separator. The low-pressure sub-cycle is formed by a gas-liquid separator, an expansion valve, an evaporator and an ejector. The compressor Dorin CD-300H was a prototype semi-hermetic reciprocating type compressor, and an inverter was used to change the compressor frequency. The gas cooler and the evaporator were counter-flow heat exchangers, which were made of copper and wound into spiral coils. In the heat exchangers, the refrigerant flowed through the inner tubes, and the water flowed through the annulus inversely. The volume of the cylinder separator was 7.4 $dm^3$. The detailed structure parameters of the experiment components are listed in Table 1. In addition, various sensors were embedded at the connecting pipelines of each device. Sensor types and accuracies are presented in Table 2. In the high-pressure sub-cycle, the $CO_2$ vapor from the separator is sucked into a compressor and compressed to a supercritical state. The supercritical $CO_2$ is cooled by the gas cooler, then high-pressure $CO_2$ enters the primary nozzle of the ejector. In the low-pressure sub-cycle, the liquid $CO_2$ is evaporated after being throttled by an expansion valve, then the low-pressure superheated $CO_2$ vapor is entrained into the ejector. The high-pressure

primary flow and low-pressure suction flow adequately mix in the ejector, and the mixed flow is discharged to the gas-liquid separator with a recovered intermediate pressure.

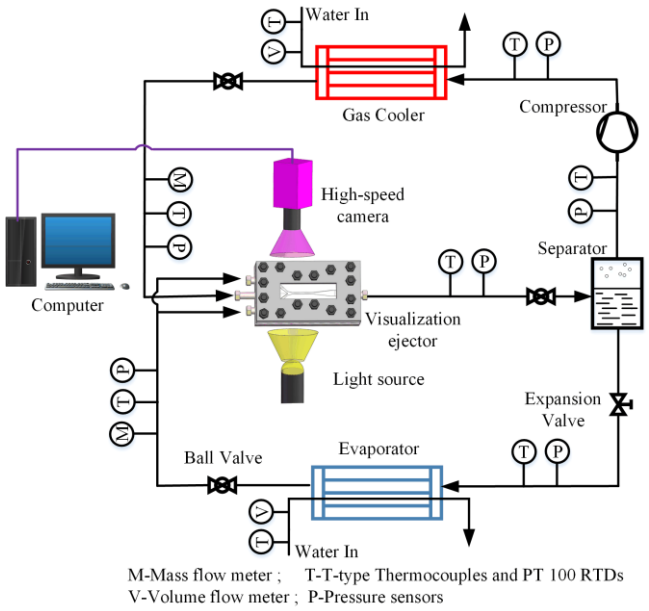


**Figure 1:** Schematic diagram of the transcritical $CO_2$ EERC

**Table 1**: Some geometric parameters of experiment components

| Component | Parameter | Value |
|---|---|---|
| Gas Cooler | Length | 10 m |
| | Internal/external diameter of inner tube | 0.006 m / 0.01 m |
| | Internal/external diameter of outer tube | 0.013 m / 0.016 m |
| Evaporator | Length | 6.0 m |
| | Internal/external diameter of inner tube | 0.007 m / 0.01 m |
| | Internal/external diameter of outer tube | 0.015 m / 0.018 m |
| Separator | Diameter | 0.164 m |
| | Height | 0.35 m |
| Compressor | Displacement | 1.46 $m^3/h$ |
| | Nominal speed | 1450 r/min |

**Table 2:** Sensors and sensor accuracy used in experimental setup

| Instrument | Range | Accuracy | Description |
|---|---|---|---|
| Coriolis mass flow meter | 0-97.2 g/s | 0.1 % Full scale | Primary flow mass flow |
| Coriolis mass flow meter | 0-69.4 g/s | 0.1 % Full scale | Suction flow mass flow |
| T-type thermocouples | -200 ºC-350 ºC | ± 0.5 ºC | $CO_2$ temperature |
| PT100 thermal resistances | 0-500 ºC | ± 0.15 ºC | Water temperature |
| Pressure sensors | 0-6 MPa | 0.075 % Full scale | Low-pressure sub-cycle |
| Pressure sensors | 0-15 MPa | 0.075 % Full scale | High-pressure sub-cycle |
| Pressure sensors | 0-20 MPa | 0.075 % Full scale | Ejector nozzle pressure |

## 2.2 Visualization Ejector

The visualization ejector is designed with a rectangular cross-section to provide a clear and undistorted optical window, as shown in Figure 2(a). It is formed by the stainless steel plate A and B, the transparent PC (polycarbonate) plate A and B, the transparent PET (polyethylene terephthalate) plate A and B with a thickness of

0.5 mm as well as an ejector stainless steel plate. Both plates are polished to ensure a good seal when assembled and pressurized. The primary flow inlet, the suction flow inlet and the outlet are placed at the stainless steel plate B, and there are four pressure measurement tubes on the stainless steel plate A to measure the pressure along the nozzle. The main component of the visualization ejector is the ejector stainless steel plate, as shown in Figure. 2(b). The dimensions of the ejector stainless steel plate are marked in Figure 2(b) and listed in Table 3.

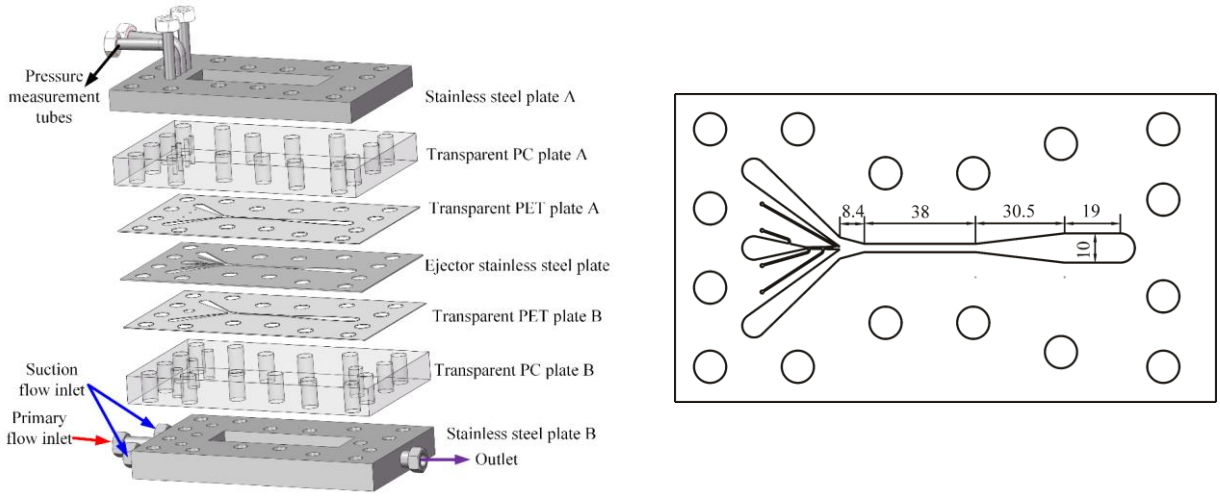


(a) Visualization ejector (b) Ejector stainless steel plate

**Figure 2:** Schematic diagram of the visualization ejector

**Table 3:** Main geometric parameters of ejector stainless steel plate

| Parameter | Value (mm) |
|---|---|
| Width of mixing chamber | 2.82 |
| Thickness | 0.78 |
| Length of converging section of nozzle | 17.85 |
| The inlet width of nozzle | 8 |
| Width of the throat | 0.49 |
| Length of diverging section of nozzle | 11.5 |
| Width of primary nozzle outlet | 0.94 |

## 2.3 Visualization Method

The direct photography method is utilized to investigate the two-phase flow in a transcritical $CO_2$ ejector. The visualization test platform is mainly formed by a high-speed camera, a visualization ejector and a light source, as shown in Figure 3. The camera is utilized to capture images with a constant frame rate of 1000 fts and connected to a computer with an Ethernet cable. A LED lamp is used to provide a light source for the camera with constant lightness.

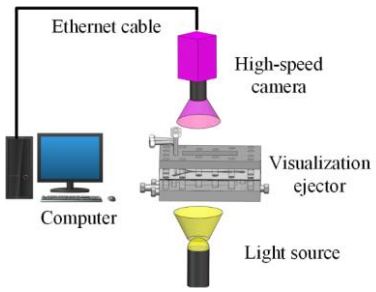


**Figure 3:** Schematic diagram of visualization test platform

The visualization principle is based on the light scattering. The light can pass the pure fluid zone straightly because of the continuity of the single-phase flow. However, the light will be scattered by the surface of small droplets or bubbles in the two-phase region. Therefore, the transmittance of the two-phase flow will be decreased, and less light enters the lens of the high-speed camera. The higher the number density of bubbles or drops, more light will be scattered, and the gray scale will be lower.

### 2.4 Pressure Measurement

Four pressure measurement points are cut on the ejector stainless steel plate by laser, as shown in Figure 4. The pressure measurement points are connected to the nozzle by four spindly channels with a width of 0.4 mm. The measurement point A is located at the converging section of the nozzle, and the axial distance from the throat is 5.75 mm. The measurement point B is slightly behind the nozzle throat by 0.6 mm to maintain the completeness of throat dimensions. The measurement point C is situated at the diverging section of nozzle, and the axial distance from the throat is 5.75 mm. The measurement point D is set before the nozzle outlet by 0.5 mm to retain the completeness of the nozzle outlet.

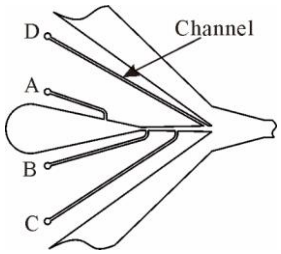


**Figure 4:** Position of pressure measurement points

## 3. RESULTS AND DISCUSSION

Primary flow inlet conditions provide the expansion motivation for the fluid, which has a direct influence on the pressure distribution and phase change position. Considering that the primary flow in the nozzle can not freely expand but is restricted by suction flow, so the suction flow inlet pressure also has an impact on the pressure distribution and phase change.

### 3.1 Effect of Primary Flow Inlet Condition

In the experiment, the primary flow inlet pressure $P_P$ decreased from 10.5 MPa to 9.0 MPa, and the primary flow inlet temperature $T_P$ reduced from 38.39 °C to 31.73 °C. The detailed operating conditions are given in Table 4.

**Table 4:** Experiment operating conditions.

| Test No. | $P_P$ (MPa) | $T_P$ (°C) | $P_S$ (MPa) | $T_S$ (MPa) |
|---|---|---|---|---|
| E1 | 10.5 | 38.39 | 4.54 | 20.02 |
| E2 | 10.0 | 35.41 | 4.19 | 22.99 |
| E3 | 9.5 | 33.32 | 3.79 | 24.35 |
| E4 | 9.0 | 31.73 | 3.24 | 24.30 |

The visualization results are presented in Figure 5. Depending on the visualization methods, the light zone and the dark zone represents the single-phase flow and the two-phase flow, respectively, and the interface is the phase change position. The profile of the nozzle and the phase change position is lined out in Figure 5. The images illuminate that the phase change position is located after the nozzle throat when primary flow inlet pressure decreases from 10.5 MPa to 9.5 MPa, as shown in line N, which is consistent with the numerical simulation results of Palacz *et al*. (2017). When continuing reducing the primary flow inlet pressure to 9.0 MPa, the phase change position moves to the upstream of the throat, as shown in Line M, which can be supported by the numerical simulation results of Haida *et al*. (2018). Therefore, the visualization experiment results indicate that the phase change position closely relates to the operating conditions, and phase change can start before or after the throat.

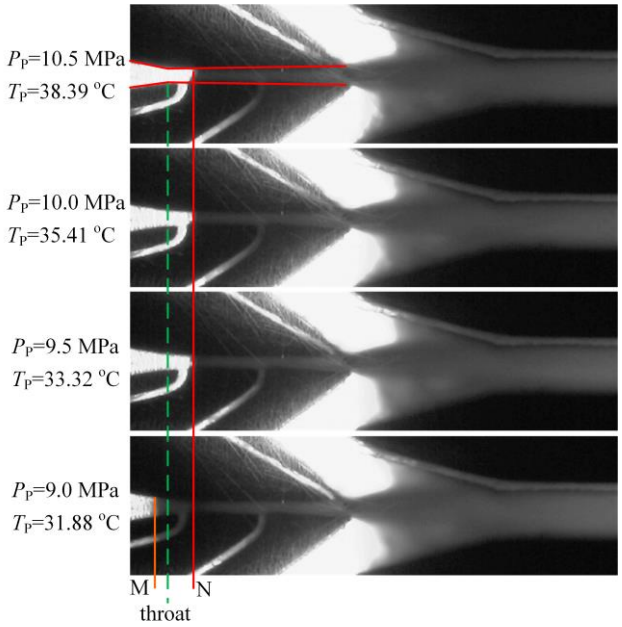


**Figure 5:** Visualization images

In order to further interpret the transition mechanism of the phase change position, it is necessary to conduct an analysis on the two-phase flow in the nozzle. The pressure distribution along the nozzle is presented in Figure 6. It is shown that the pressure of point B is higher than the $CO_2$ critical pressure (7.3773 MPa) when primary flow inlet pressure equals 10.5 MPa and 10.0 MPa, which indicates that the phase change occurs behind the throat. When primary flow inlet pressure reduces to 9.5 MPa and 9.0 MPa, the throat pressure is lower than the critical pressure, which is difficult to judge the thermodynamic state of the fluid in the throat, because the fluid may be the subcooled liquid. Therefore, it is essential to conduct a thermodynamic analysis. The two-phase flow in the $CO_2$ nozzle is caused by the rapid expansion of the primary flow, and the expansion process can at least theoretically approach the isentropic process (Elbel and Lawrence, 2016). Therefore, the isentropic expansion assumption and the nozzle pressure distribution were used to investigate the expansion process. Considering the throat pressure is important to determine the flow state of throat, the throat pressure is extrapolated by lineally interpolating with the pressure of point A and point B, as shown in Figure 6. It should be noted that the linearly extrapolated throat pressure may be slightly lower than the actual throat pressure, because the throat owns the smallest area which will cause a bigger pressure drop.

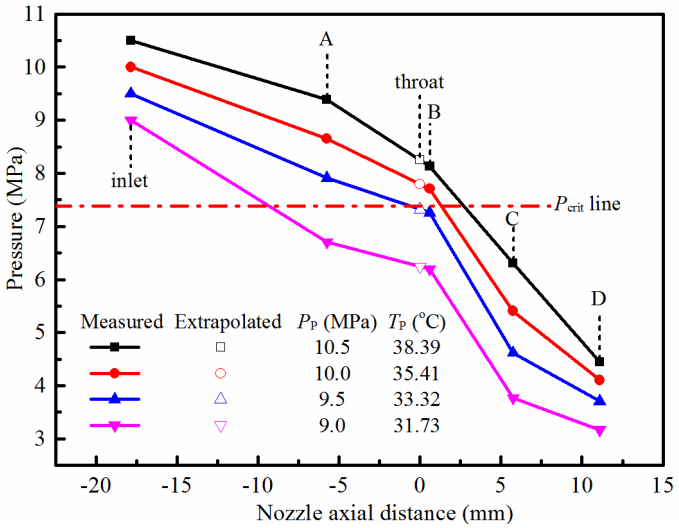


**Figure 6:** Pressure distribution along the nozzle

The thermodynamic analysis is conducted by comparing the isentropic temperature with the saturation temperature. The phase change will start when the isentropic temperature equals the saturation temperature, because the flow enters the two-phase region from the sub-cooled liquid region. The isentropic temperature is calculated with the pressure and the primary flow inlet specific entropy which is looked up with the primary flow inlet pressure and temperature from the REFPROP V8.0 software. The saturation temperature is looked up with the pressure. The comparison results are shown in Figure 7. When primary flow inlet pressure equals 10.5 MPa, it is visible that the isentropic temperature of point B is higher than the $CO_2$ critical temperatrure (30.978 ºC). The isentropic temperature and the saturation temperature are identical at the point C, which indicates that the phase change starts between the point B and point C. When the primary flow inlet pressure equals 10.0 MPa, there is no saturation temperature in point B meaning that the pressure of point B is higher than the critical pressure. The coincident point of temperature is located at the point C, indicating that the flow enters the two-phase region already. When the primary flow inlet pressure reduces to 9.5 MPa, the saturation temperature of throat is higher than the corresponding isentropic temperature, which reveals that the fluid of throat is the subcooled liquid. The coincident point of temperature is located at the point C, indicating that the sub-cooled $CO_2$ liquid evaporates between the throat and the point C. When $P_P$ continues decreasing to 9.0 MPa, the coincident point of temperature moves upstream to the throat, but the saturation temperature of point A is higher than corresponding isentropic temperature, which implies that the phase change occurs between the point A and the throat. The isentropic expansion analysis reveals that the flow of throat is supercritical stream when primary inlet pressure is higher than 10.0 MPa, so the phase change starts after the throat. When the primary flow inlet pressure decreases to 9.5 MPa, the flow of throat becomes the sub-cooled liquid which results in the delayed phase change at the throat. When further reducing the primary flow inlet pressure to 9.0 MPa, the fluid of throat is gas-liquid two-phase flow, indicating that the phase change begins before the throat. The variation of the flow state of throat may be caused by the decrease of the primary flow inlet specific entropy. Moreover, the analyzed phase change position agrees well with the visualization images.

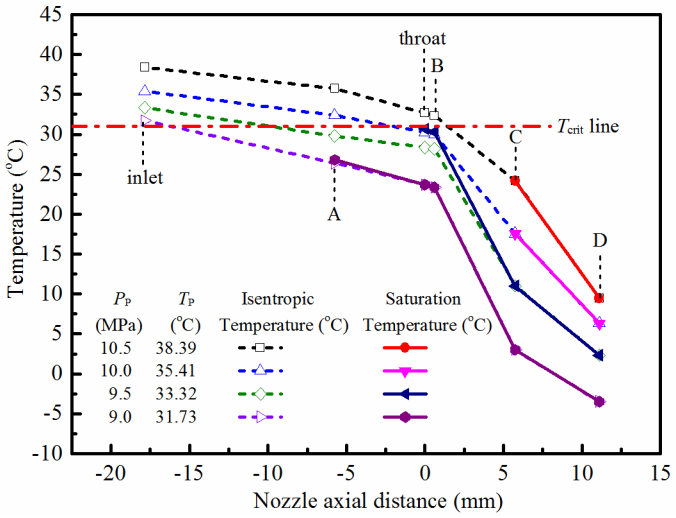


**Figure 7:** Comparison of isentropic temperature and saturation temperature

### 3.2 Effect of Suction Flow Inlet Pressure

In the following experiment, the primary flow inlet pressure $P_P$ was maintained to 10.5 MPa, and the suction fluid inlet pressure $P_S$ varied from 4.62 MPa to 3.72 MPa. The detailed operating conditions are shown in Table 5.

**Table 5:** Experiment operating conditions.

| Test No. | $P_P$ (MPa) | $T_P$ (ºC) | $P_S$ (MPa) | $T_S$ (MPa) |
|---|---|---|---|---|
| E5 | 10.50 | 38.0 | 4.62 | 23.46 |
| E6 | 10.50 | 36.7 | 4.47 | 23.41 |
| E7 | 10.51 | 36.9 | 4.27 | 24.87 |
| E8 | 10.52 | 36.4 | 4.0 | 25.43 |

| | | | | |
|---|---|---|---|---|
| E9 | 10.51 | 35.7 | 3.89 | 25.46 |
| E10 | 10.50 | 35.1 | 3.72 | 25.66 |

The pressure distribution curves for different suction flow inlet pressure are shown in Figure 8. The pressure profile indicates that the pressure drop gradient in the convergent section of the nozzle increases as the suction flow inlet pressure decreases. In order to figure out the reason of this variation, the expansion degree of the primary flow was investigated by comparing the expansion angle at the nozzle outlet, as shown in Figure 9. It shows that the expansion angle increases as the suction flow inlet pressure decreases, which means that the primary flow expands more fully by relaxing the restriction of suction flow. Therefore, the pressure difference between the convergent section of the nozzle increases as the suction flow inlet pressure decreases.

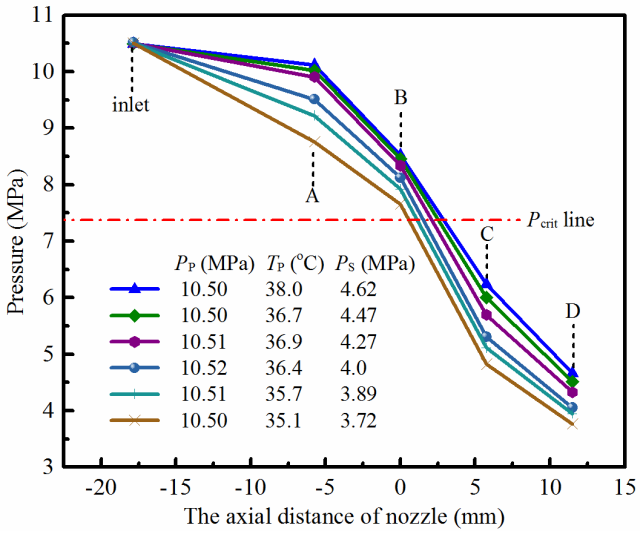


**Figure 8:** Pressure distribution along the nozzle

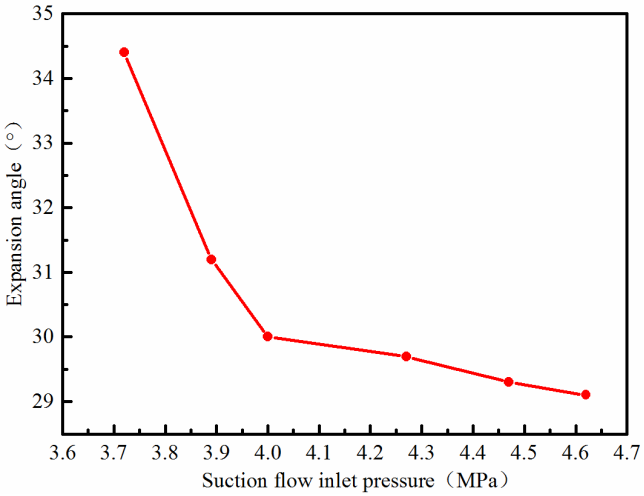


**Figure 9:** Expansion angle of primary flow

In addition, corresponding visualization images for various suction flow inlet pressure are shown in Figure 10. The images demonstrate that the phase change position is located at the rear of the throat for all current operating conditions, because the measured pressure of point B is higher than the $CO_2$ critical pressure (7.3773 MPa), as illustrated in Figure 8. According to the visualization principle, the gray value of the image is linked to the number density of bubbles, so the phase change position can be located with the gray value distribution. That is, there exists a steep decrease of gray value when phase change starts. In order to quite precisely discriminate the difference of the images, the gray value curves along the nozzle centerline are extracted with the built-in functions of the

MATLAB software when the suction flow inlet pressure equals 4.62 MPa and 3.72 MPa, as shown in Figure 11. The MATLAB function "impixelinfo" is used to obtain the pixel coordinates of the images, and the function "rgb2gray" is utilized to acquire the gray values of pixels. When the suction flow inlet pressure is equal to 3.72 MPa, the rapid decline of gray value precedes that when the suction flow inlet pressure equals 4.72 MPa, which manifests that the corresponding phase change position moves upstream as the suction flow inlet pressure decreased. Under the experimental operating conditions, the phase change position moved forward by about 0.5 mm as the suction flow inlet pressure decreased from 4.62 MPa to 3.72 MPa.

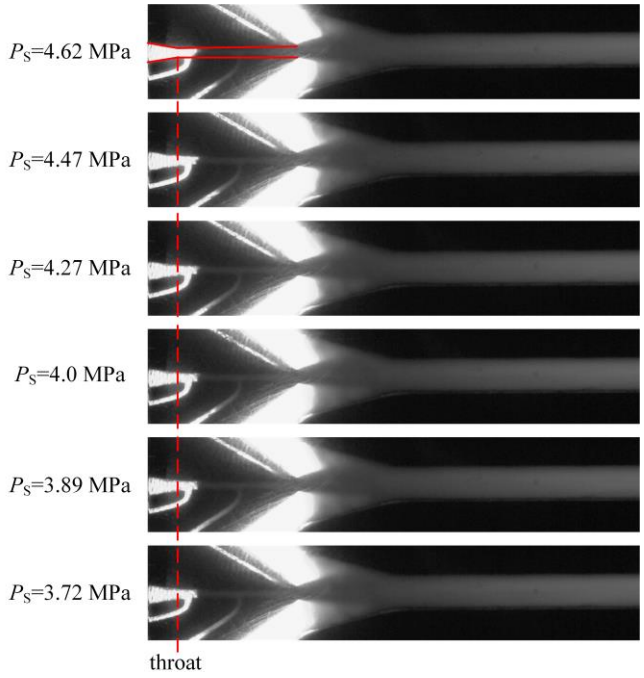


**Figure 10:** Visualization images for various suction flow inlet pressure ($P_P$=10.5 MPa)

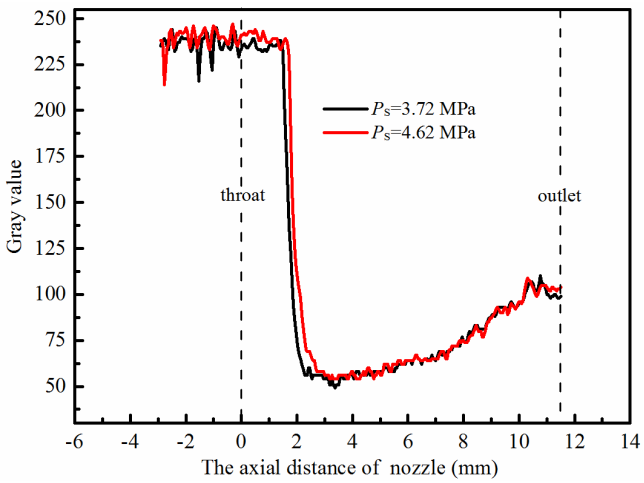


**Figure 11:** Gray value along the nozzle

## 4. CONCLUSIONS

Based on the high-speed photography technology, a visualization experiment research on a transcritical $CO_2$ two-phase ejector was performed to record the phase change phenomena and measure the pressure distribution in the primary converging-diverging nozzle under different operating conditions. The images showed that the phase change could start before and after the throat, and the position moved upstream as primary flow inlet pressure and

temperature decreased. The same tendency was observed as the suction flow inlet pressure decreased as keeping the primary flow inlet pressure constant. The phase change position was explained by the pressure distribution and the isentropic expansion assumption, and the analyzed results were consistent with the images. Moreover, the pressure distribution demonstrated that the pressure differences in the convergent section of the nozzle increased as the suction flow inlet pressure decreased due to the decreasing restriction of the primary flow expansion.

## NOMENCLATURE

| | | |
|---|---|---|
| *P* | pressure | (MPa) |
| *T* | temperature | (°C) |

**Subscript**

| | |
|---|---|
| P | primary flow |
| S | suction flow |
| crit | critical point |

## REFERENCES


Elbel, S., Lawrence, N. (2016). Review of recent developments in advanced ejector technology. *Int. J. Refrig.*, *62*, 1-18.

Besagni, G., Mereu, R., Inzoli, F. (2016). Ejector refrigeration: A comprehensive review. *Renew. Sustain. Energy Rev.*, *53*, 373-407.

Li, D. Q., Groll, E. A. (2004). Transcritical $CO_2$ refrigeration cycle with ejector-expansion device. *Int. J. Refrig.*, *28*(5), 766-773.

Deng, J. Q., Jiang, P. X., Lu, T., Lu, W. (2007). Particular characteristics of transcritical $CO_2$ refrigeration cycle with an ejector. *Appl. Therm. Eng.*, *27*(2), 381-388.

Ahammed, M. E., Bhattacharyya, S., Ramgopal, M. (2014). Thermodynamic design and simulation of a $CO_2$ based transcritical vapour compression refrigeration system with an ejector. *Int. J. Refrig.*, *45*, 177-188.

Elbel, S., Hrnjak, P. (2008). Experimental validation of a prototype ejector designed to reduce throttling losses encountered in transcritical R744 system operation. *Int. J. Refrig.*, *31*(3), 411-422.

Lee, J. S., Kim, M. S., Kim, M. S. (2011). Experimental study on the improvement of $CO_2$ air conditioning system performance using an ejector. *Int. J. Refrig.*, *34*(7), 1614-1625.

Liu, F., Li, Y., Groll, E. A. (2012). Performance enhancement of $CO_2$ air conditioner with a controllable ejector. *Int. J. Refrig.*, *35*(6), 1604-1616.

Bouhanguel, A., Desevaux, P., Gavignet, E. (2011). Flow visualization in supersonic ejectors using laser tomography techniques. *Int. J. Refrig.*, *34*(7), 1633-1640.

Rao, S. M. V., Jagadeesh, G. (2014). Observations on the non-mixed length and unsteady shock motion in a two dimensional supersonic ejector. *Phys. Fluids*, *26*(3), 243-247.

Little, A. B., Garimella, S. (2016). Shadowgraph visualization of condensing R134a flow through ejectors. *Int. J. Refrig.*, *68*, 118-129.

Zhu, Y. H., Wang, Z. C., Yang, Y. P., Jiang, P. X. (2017). Flow visualization of supersonic two-phase transcritical flow of $CO_2$ in an ejector of a refrigeration system. *Int. J. Refrig.*, *74*, 354-361.

Nakagawa, M., Berana, M. S., Kishine, A. (2009). Supersonic two-phase flow of $CO_2$ through converging–diverging nozzles for the ejector refrigeration cycle. *Int. J. Refrig.*, *32*(6), 1195-1202.

Elbel, S. (2011). Historical and present developments of ejector refrigeration systems with emphasis on transcritical carbon dioxide air-conditioning applications. *Int. J. Refrig.*, *34*(7), 1545-1561.

Palacz, M., Haida, M., Smolka, J., Nowak, A. J., Banasiak, K., Hafner, A. (2017). HEM and HRM accuracy comparison for the simulation of $CO_2$ expansion in two-phase ejectors for supermarket refrigeration systems. *Appl. Therm. Eng.*, *115*, 160-169.

Haida, M., Smolka, J., Hafner, A., Palacz, M., Banasiak, K., Nowak, A. J. (2018). Modified homogeneous relaxation model for the R744 trans-critical flow in a two-phase ejector. *Int. J. Refrig.*, *85*, 314-333.


## ACKNOWLEDGEMENT

This work was supported by the National Natural Science Foundation of China (Grant No. 51676148).